RESEARCH ARTICLE

Optimization of an Air Pressure System: A Multi-Objective Control and Modeling Approach

VÍCTOR HUILCAPI[1], CHRISTIAN CASTILLO[2], DANIEL SANCHEZ[2], AND RICARDO CAJO[2]

[1]Facultad de ingenierías, Universidad Politécnica Salesiana, Guayaquil 090109, Ecuador
[2]Facultad de Ingeniería en Electricidad y Computación, Escuela Superior Politécnica del Litoral, ESPOL, Campus Gustavo Galindo, Guayaquil 9000, Ecuador

Corresponding author: Víctor Huilcapi (vhuilcapi@ups.edu.ec)

ABSTRACT This paper presents the application of a methodological approach based on multi-objective optimization for identifying a nonlinear model and designing controllers for an air pressure system. First, the parameters of the system's nonlinear model are determined based on experimental data obtained from the process. Subsequently, the methodology is extended to tuning cascade PI controllers, where experimental tests are performed in the laboratory. This methodology allows a designer to have a detailed view of the proposed multi-objective problem (both in the modeling and controlling the air pressure system). Depending on the level of detail required, the design objectives of the multi-objective problem are proposed. In this case, two objectives are proposed to evaluate the model's performance and three objectives for evaluating the control system's quality. Among the advantages offered by this methodology is the easy understanding of the conflicts that arise between the design objectives, which allows for selecting an optimal solution according to the preferences established by a designer and based on detailed information on the system's performance. In this case, a conflict between the dynamics of the pressures of the air pressure system could be evidenced, both in the modeling and in the control. The proposed methodology also allows the analysis of the behavior of the air pressure system in a global framework without loss of information, which would not be feasible in a traditional single-objective analysis that agglutinates all the information in a single design objective. Although the decision-making stage of the proposed methodology is more complex than a single-objective analysis, it is justified as it provides detailed and complete information to a designer to make accurate and effective decisions on how to model and control the compressed air pressure system effectively.

INDEX TERMS Air pressure systems, multi-objective optimization methodology, multi-objective evolutionary algorithm (*ev*-MOGA), level diagram (LD), cascade PI controller, nonlinear model, decision-making processes.

I. INTRODUCTION

The air pressure systems are commonly used in various applications such as compressed air energy storage, pneumatic actuation, and air-powered tools. These systems involve storing air under pressure in tanks or vessels to provide a reliable and versatile energy source for various processes. For

The associate editor coordinating the review of this manuscript and approving it for publication was Xiwang Dong.

example, air pressure systems drive pneumatic actuators and cylinders in automation processes, enabling precise and controlled movement of components and machinery. Therefore, control algorithms play a crucial role in ensuring efficiency and safety in various industrial processes and applications [1], [2], [3]. Several control approaches for air tank pressure systems have been widely studied and applied in various industrial and engineering domains. For example, in [4], a practical method for implementing a proportional-integral-derivative

(PID) controller for compressed air pressure systems by applying a set of experimental tuning rules and a frequency domain system analysis is proposed. The authors provide a PID tuning rule specifically tailored for pressure control applications in fluid power systems. The proposed rule considers the system dynamics and aims to achieve optimal performance regarding disturbance rejection and set-point tracking. The experimental results support the effectiveness of the proposed tuning rule, highlighting its advantages over other methods. A variable universal fuzzy PID controller for a multi-level gas tank system is proposed by Zhang et al. [5]. Five controllers are designed based on desired pressures and compared with conventional PID control. Simulation results exhibit improved pressure dynamics using variable universal fuzzy PID control, reducing overshoot and response time. The study demonstrates successful pressure regulation and suggests potential extensions for more complex systems with disturbances.

On the other hand, advanced control techniques have been studied for air tank pressure systems, such as generalized predictive control (GPC), fuzzy supervisory control, robust control, multi-objective evolutionary algorithms (MOEA), fractional control techniques, etc. The work presented in [6] addresses challenges in controlling a three-level air tank system due to time delay and inertia. A constrained generalized predictive control (GPC) algorithm is proposed, utilizing recursive least squares for parameter identification and Diophantine equations for prediction modeling. The quadratic programming-based rolling optimization strategy enhances control law calculation. The experimental comparison demonstrates the superior effectiveness of the approach over PID and unconstrained GPC methods, reducing overshoot, vibration, and settling time while improving control performance. An optimization model for compressor station scheduling, employing a constrained multi-objective evolutionary algorithm named CMOEA/D-CDP to tackle multi-objective problems is proposed in [7]. It proposes a novel encoding scheme to simplify decision variables and mitigate complexities. The results offer a set of Pareto optimal solutions for production guidance. Case studies indicate the superiority of the proposed encoding over conventional methods, highlighting challenges with different compressor types. However, the conclusion calls for further exploration using different CMOEAs. The paper provides valuable insights but requires broader validation across diverse algorithms for comprehensive assessment and applicability. Another paper introduces a fuzzy supervisory control system for pressure processes using integral-based identification [8]. This method enhances robustness to noise, with theoretical analysis and experimental validation showing improved performance over constant PID gains designed by pole placement. The work presented by Bingi1 et al [9] introduces the 2DOF-FOPID controller for real-time pressure process control, highlighting its advantages over conventional PID controllers. It emphasizes improved set-point tracking and disturbance rejection capabilities, substantiated

by experimental results showing superior performance in overshoot reduction and faster settling time. Parameter tuning and controller conversion methods are outlined, enhancing applicability in parallel and series configurations. However, the assessment of disturbance rejection across compared controllers lacks depth. The proposed adaptation algorithm for parameter tuning is an intriguing suggestion for future enhancement.

Finally, Velmurugan et al. [10] explores the robust performance of a fractional first-generation controller for an air pressure system, achieving linear behavior in a nonlinear system. Controller performance is evaluated using error and time indices for three operating points, showing that it outperforms conventional controllers. Based on the literature described previously in this article, the modeling and control of an air pressure system are proposed by applying a multi-objective design procedure (MOOD). In the optimization stage, an *evolutionary multi-objective genetic algorithm ev*-MOGA was applied [11], [12] and in the stage of visualizing Pareto fronts for decision-making, the *Level Diagram (LD)* tool was used, [13]. Further details about the multi-objective design procedure applied in this article are shown in section II. The main contributions of this research are outlined below:

- A multi-objective design approach is shown as a real application of [14] for the modeling and control of an experimental air pressure system.
- Through the integration of *ev*-MOGA and the *LD*, a robust decision-making framework is introduced for the visualization of multidimensional Pareto fronts.
- A multidimensional analysis of the conflicts or trade-offs that typically occur between design objectives in real engineering problems with the goal of keeping a designer sufficiently informed to make right decisions.
- Extensive laboratory and simulation tests have been carried out to show the reliability and effectiveness of the proposed multi-objective methodology in process modeling and control.

The paper is organized into several key sections. It begins with a comprehensive exploration in Section II, delving into the fundamentals of multi-objective optimization, providing a robust theoretical foundation. Section III focuses on elucidating the model of the didactic pressure regulator (RT 450.03), offering a clear understanding of the system under study. Sections IV and IV-A elaborate on applying a multi-objective identification approach to the air pressure system, detailing the optimization techniques employed for system model identification. Furthermore, Section IV-B extends this optimization methodology to the fine-tuning of system controllers. The pivotal findings and discussions arising from this approach are encapsulated in Section V, elucidating the results and engaging in insightful discussions. Finally, Section VI encapsulates the paper with conclusive remarks and implications drawn from the conducted research, providing a structured closure to the study.

II. FUNDAMENTALS OF MULTI-OBJECTIVE OPTIMIZATION

In real engineering applications, it is very common to find problems that require the optimization of multiple design objectives simultaneously. Generally, these design objectives are also in conflict (meaning that improving some entails worsening others) and subject to physical constraints. Multi-objective optimization techniques are advisable to solve these problems [14], [15], [16].

A multi-objective optimization design generally consists of at least three stages: 1) the definition of the multi-objective problem (MOP); 2) the multi-objective optimization process; and 3) the multicriteria decision stage [17], [18].

According to [11], [19], and [20], a multi-objective optimization problem (stage 1) can be defined as shown in (1)-(5).

$$\min_{x \in D} J(x) \tag{1}$$

$$J(x) = \{J_1(x), J_2(x), \ldots, J_s(x)\} \tag{2}$$

$$\text{subject to: } g(x) \leq 0 \tag{3}$$

$$h(x) = 0 \tag{4}$$

$$\underline{x} \leq x_i \leq \overline{x}, i = [1, \ldots, n] \tag{5}$$

where, $x = (x_1, x_2, \ldots x_n) \in R^n$ represent the decision vector; D is the decision space; $J(x) \in R^m$ is the design objectives vector; $g(x)$, $h(x)$ are the constraint vectors; y $\underline{x}, \overline{x}$ are the upper and lower bounds of the decision space. Therefore, from a multi-objective perspective, there is not a single optimal solution to a problem but rather a set of optimal solutions (where none is better than another) with different trade-offs among the design objectives. This set of optimal solutions forms what is known as the Pareto front [19], [21]. The optimal Pareto set is based on the definition of Pareto dominance proposed in [22] and [23]. The definitions of dominance, Pareto set, and Pareto front are schematized in Figure 1 and shown in (6), (7), (8) respectively.

Definition 1 (Dominance [22], [23]): A vector $\mathbf{x}^1$ dominates another vector $\mathbf{x}^2$, (denoted by $\mathbf{x}^1 \preceq \mathbf{x}^2$), if $J(\mathbf{x}^1)$ is not worse than $J(\mathbf{x}^2)$ in all design objectives, and it is better in at least one objective.

$$\forall i \in A := [1, \ldots, s], J_i(\mathbf{x}^1) \leq J_i(\mathbf{x}^2) \wedge \exists i \in A : J_i(\mathbf{x}^1) < J_i(\mathbf{x}^2) \tag{6}$$

Definition 2 (Pareto Set [23]): The Pareto set (denoted by $\mathbf{X}_p$) is the set of solutions in D not dominated by other solutions in D and defined by:

$$\mathbf{X}_p := \{\mathbf{x} \in D | \nexists \mathbf{x}' \in D : \mathbf{x}' \preceq \mathbf{x}\} \tag{7}$$

Definition 3 (Pareto Front [23]): Given the Pareto set $\mathbf{X}_p$, the Pareto front $J(\mathbf{X}_p)$ is defined by:

$$J(\mathbf{X}_p) := \{J(\mathbf{x}) | \mathbf{x} \in \mathbf{X}_p\} \tag{8}$$

In Figure 1 (a), the Pareto front $J(\mathbf{X}_p)$ of a multi-objective optimization problem with two design objectives, $J_1(\mathbf{x})$ and
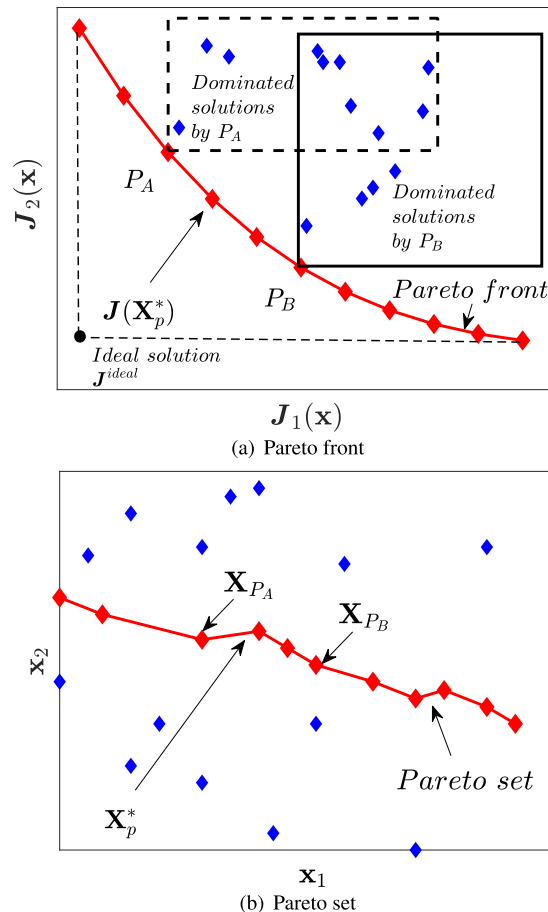

(a) Pareto front

(b) Pareto set

FIGURE 1. Notion of Pareto front and Pareto set in a MOP with two dimensions.

$J_2(\mathbf{x})$, is depicted in red. Figure 1 (b) illustrates the decision space with its decision variables $\mathbf{x}_1$ and $\mathbf{x}_2$ (The solutions in red constitute the Pareto set).

The solutions shown with red diamonds in Figure 1 (a) are non-dominated, as there are no other solutions within the Pareto front that are better in all design objectives. On the contrary, the red ones dominate the solutions shown in blue diamonds. Therefore, they are not part of the Pareto front. The solutions in red in Figure 1 (b) are Pareto optimal, as their corresponding design objectives are on the Pareto front.

In the multi-objective optimization stage (stage 2), it is necessary to choose an optimization algorithm that satisfactorily obtains the approximations of the Pareto fronts of each MOP [24], [25].

Multi-objective optimization algorithms aim to find a set of solutions $\mathbf{X}_p^* \subset \mathbf{X}p$, such that $J(\mathbf{X}_p^*)$ satisfactorily characterizes $J(\mathbf{X}_p)$. Sometimes, $J(\mathbf{X}_p)$ may be infeasible to obtain if it has infinite solutions.

It is essential to mention that $\mathbf{X}_p^*$ is not a unique set. When obtaining a set $\mathbf{X}_p^*$, a designer can select a solution according to their preferences, for example, by choosing the solution closest to the ideal solution (utopian solution $\mathbf{J}^{ideal}$, which

minimizes each design objective of a MOP, as shown in Figure 1).

Currently, various optimization algorithms use different techniques to approximate the Pareto front [26], [27], [28]. Among the most used optimization techniques are evolutionary techniques, which have had remarkable development and application in solving increasingly complex multi-objective optimization problems [29], [30], [31]. A significant example of these techniques is multi-objective evolutionary algorithms (MOEAs), successfully applied to many real engineering problems [12], [32], [33].

Multi-objective genetic algorithms (MOGA) can be considered the most applicable representatives [34], [35]. These algorithms have been used to solve various optimization problems with satisfactory results [20], [36], [37].

In this paper, the *ev*-MOGA algorithm was used to obtain the Pareto fronts of the MOP [11], [38]. The *ev*-MOGA algorithm is an elitist multi-objective evolutionary algorithm, where two sub-populations evolve simultaneously and iteratively to achieve effective convergence to the Pareto front.

After the optimization algorithm calculates an approximation of the Pareto front $J(\mathbf{X}_p^*)$, it is necessary to analyze the features of the solutions that form this front $J(\mathbf{X}_p^*)$ (stage 3). The objective of conducting a detailed analysis of the front is to offer the best solution to the MOP according to the designer's preferences. For this purpose, Pareto front visualization tools are handy and powerful. Therefore, they have been widely accepted to assist a designer in selecting optimal solutions from a Pareto front [39], [40], [41].

In this work, the multidimensional Pareto front visualization tool called *Level Diagram* was used to analyze the solutions of each MOP [13]. The *Level Diagram* has interesting features such as easy analysis of solutions on the fronts (interaction with colors, highlighting solutions, exporting data, etc.) and ease of generating or incorporating various viewpoints on the Pareto fronts, since it allows working with different synchronized norms.

In Figure 2 (a), a Pareto front of a bi-dimensional MOP is shown traditionally, and in Figure 2 (b), its representation using LD is demonstrated. Three points (A, B, C) have been taken on each Pareto front to show their equivalences. For example, Point A in Figure 2 (a) represents the solution with the best performance for objective $J_1(\mathbf{X})$ and the worst performance for $J_2(\mathbf{X})$. Figure 2 (b) represents each design objective in a separate graph. Therefore, point A is located on the left for objective $J_1(\mathbf{X})$ and on the right for $J_2(\mathbf{X})$.

III. MODEL OF THE DIDACTIC PRESSURE REGULATOR

The RT 450.03 pressure regulation module consists of two steel pressure vessels and uses compressed air as its working fluid, as shown in Figure. 3.

Both tanks are provided with a pressure gauge and an overpressure valve, and the B2 tank also has an evacuation valve. The two tanks communicate with each other through
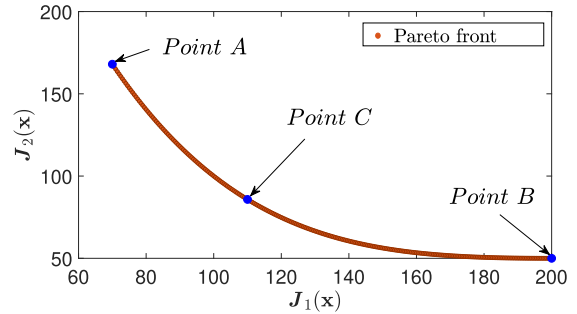
(a) Classical representation of a two-dimensional Pareto front
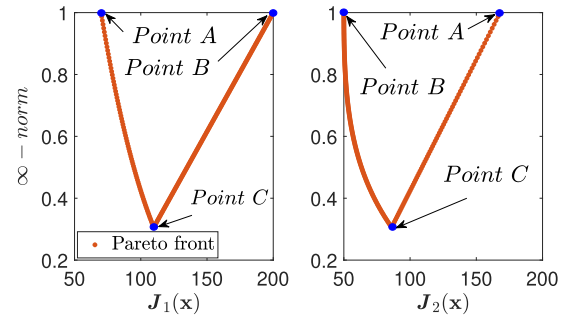
(b) Representation of a two-dimensional Pareto front using LD with $\infty -$ *norm*

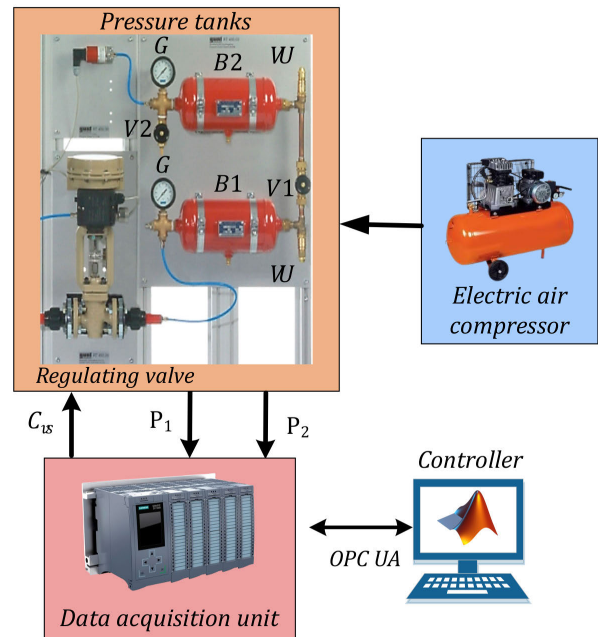**FIGURE 2.** Representation of Pareto fronts using *Level Diagram*.

FIGURE 3. Components of the air pressure system.

a vent valve, so they are connected in series. In this way, a second-order pressure regulation system can be represented.

The components of the RT 450.03 pressure regulation module are $V1$, $V2$, G, and VU (see Figure 3). The details of the components are shown below.

- $B1$, $B2$: Pressure vessels
- $V1$: Vent valve

- $V2$: Evacuation valve
- G: Pressure gauge
- VU: Overpressure valve

To describe the behavior of the compressed air system, we start with a dynamic state mass balance for each tank described as shown in (9)-(10).

$$Q_1(t) - Q_2(t) = \frac{dm_1(t)}{dt} \quad (9)$$

$$Q_2(t) - Q_3(t) = \frac{dm_2(t)}{dt} \quad (10)$$

On the other hand, the flow rate in the valves can be described as shown in (11).

$$Q_1(t) = K_s C_{vs}\sqrt{(P_s - P_1)\rho}$$
$$Q_2(t) = K_2 C_{v2}\sqrt{(P_1 - P_2)\rho}$$
$$Q_3(t) = K_3 C_{v3}\sqrt{(P_1 - P_3)\rho} \quad (11)$$

where, $m_1(t)$ and $m_2(t)$ are the masses of the gas in each tank, if the pressure in the tank is low, the relationship between the mass of the gas and the pressure is established by the equation of state for ideal gases shown in (12).

$$P(t) = \frac{RT}{VM}m(t) \quad (12)$$

where, T is the absolute temperature in the tank, V is the tank volume, M is the molecular weight of the gas and R is the ideal gas constant.

Finally, the equations governing the dynamic behavior of pressures in each tank as a function of changes in the percentage of the opening of the control valve are:

$$K_s C_{vs}\sqrt{(P_s - P_1)\rho} - K_2 C_{v2}\sqrt{(P_1 - P_2)\rho} = \frac{V_1 M}{RT_1}\frac{dP_1(t)}{dt} \quad (13)$$

$$K_2 C_{v2}\sqrt{(P_1 - P_2)\rho} - K_3 C_{v3}\sqrt{(P_1 - P_3)\rho} = \frac{V_2 M}{RT_2}\frac{dP_2(t)}{dt} \quad (14)$$

where K_s, K_2, and K_3 are adjustment constants for the conductance coefficients of the valves.

The parameters considered for the nonlinear model for the air pressure system are summarized in Table 1.

IV. MULTI-OBJECTIVE IDENTIFICATION APPROACH APPLIED TO THE AIR PRESSURE SYSTEM

A. MULTI-OBJECTIVE OPTIMIZATION FOR SYSTEM MODEL IDENTIFICATION

When defining the multi-objective optimization problem for system identification, it is necessary to consider the parameters identified in the proposed model (9)-(14). In addition to the system's initial conditions, the constraints of the MOP and the optimality criterion applied to represent the Pareto front. For this application, the criteria defined in (15)-(20) were established, where the average errors of pressures P_1 and P_2 of each tank in the system are evaluated. The experiment was conducted for 1000 seconds, taking the plant through

TABLE 1. System parameters.

Variable	Description	Units
P_s	Compressor pressure	atm
P_1	Tank 1 pressure	atm
P_2	Tank 2 pressure	atm
ρ	Air density	1.29 g/l
R	Ideal gas constant	$0.082 \frac{atm.l}{K.mol}$
M	Molecular weight of the gas	$28.97 \frac{g}{mol}$
T_1	Tank 1 temperature	$^\circ K$
T_2	Tank 2 temperature	$^\circ K$
V_1	Tank 1 volume	l
V_2	Tank 2 volume	l
C_{vs}	Control valve opening percentage	%
C_{v2}	Opening percentage for valve 2	%
C_{v3}	Opening percentage for valve 3	%
Q_1	Tank 1 inlet flow	g/s
Q_2	Tank 2 inlet flow	g/s
Q_3	Outflow	g/s

TABLE 2. Bounds of the decision vector x_m for system model identification.

	Bounds of x_m		
$\mathbf{x}_m$	K_s	K_2	K_3
$\underline{\mathbf{x}}_m$	0.01	0.01	0.01
$\overline{\mathbf{x}}_m$	10	10	50

TABLE 3. Bounds of the decision vector x_c for system control.

	Bounds of x_c			
$\mathbf{x}_c$	K_{p1}	K_{i1}	K_{p2}	K_{i2}
$\underline{\mathbf{x}}_c$	0.1	0.1	0.1	0.1
$\overline{\mathbf{x}}_c$	100	100	100	100

different operating ranges, and 10000 samples were acquired ($N = 10000$).

$$\min_{x_m \in D} J(x_m) \quad (15)$$

$$J(x_m) = \{J_1(x_m), J_2(x_m)\} \quad (16)$$

$$J_1(x_m) = \frac{1}{N}\sum_{k=1}^{N}|P_{1\ experimental}(k) - P_{1\ identified}(k)| \quad (17)$$

$$J_2(x_m) = \frac{1}{N}\sum_{k=1}^{N}|P_{2\ experimental}(k) - P_{2\ identified}(k)| \quad (18)$$

The decision vector is represented by:

$$x_m = \{K_s, K_2, K_3\} \quad (19)$$

$$\underline{\mathbf{x}}_m \leq \mathbf{x}_m \leq \overline{\mathbf{x}}_m \quad (20)$$

where, $\underline{\mathbf{x}}_m$ and $\overline{\mathbf{x}}_m$ were established taking into consideration the technical information of the system valves provided by the manufacturer (see Table 2).

B. MULTI-OBJECTIVE OPTIMIZATION FOR TUNING SYSTEM CONTROLLERS

To control the pressures P_1 and P_2 of the nonlinear compressed air system, a cascade control structure was implemented as shown in Figure 4 (see the video of the system control at https://www.youtube.com/watch?v=AQaUshBU57I).
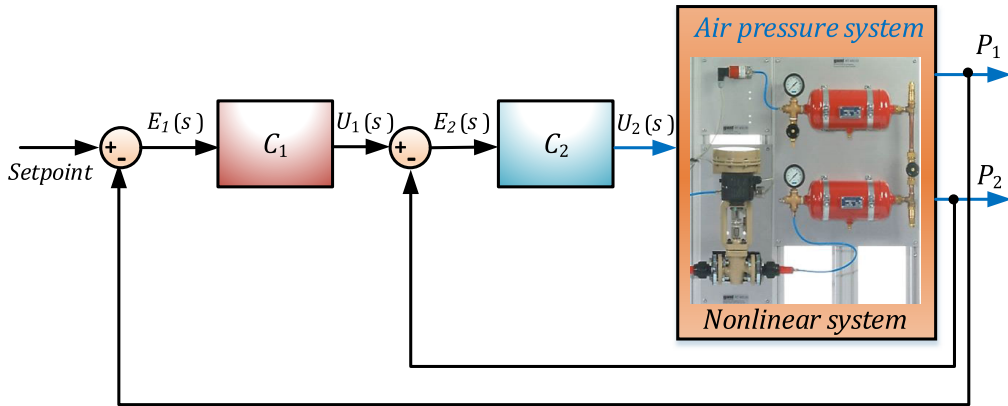
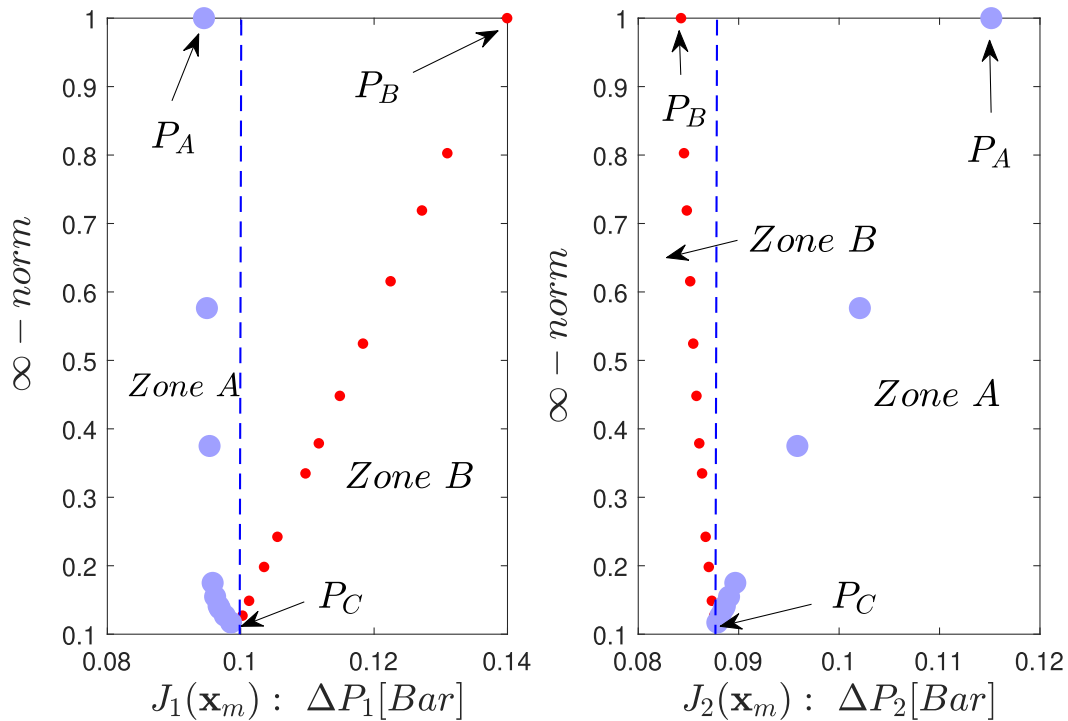**FIGURE 4.** Air pressure system control structure.

FIGURE 5. Pareto front representation of air pressure system models.

The control structure employs two proportional-integral (PI) controllers, as depicted in (21)-(22).

$$U_1(s) = \left(K_{p1} + K_{i1}\frac{1}{s}\right)E_1(s) \tag{21}$$

$$U_2(s) = \left(K_{p2} + K_{i2}\frac{1}{s}\right)E_2(s) \tag{22}$$

where, (K_{p1}, K_{i1}) and (K_{p2}, K_{i2}) represent the proportional and integral gains of the PI controllers for pressures P_1 and P_2, respectively.

For the tuning of the system controllers, optimization criteria such as the Integrated Absolute Error (IAE) and the Integral of the absolute value of the derivative control signal

(IADU) were used. The IAE index is applied to evaluate the quality of each controller for monitoring an input reference signal, while the IADU allows evaluating the quality of the control effort applied to the system.

Each MOP was proposed to find the tuning parameters of each proposed controller (K_{p1}, K_{i1}, K_{p2}, K_{i2}) as shown in (23)-(27). Each PI controller is tuned to track a step type input reference of 2 [Bar] in amplitude. The signal sampling period is ($T_s = 0.1$ s) and throughout the experiment, 10000 samples were acquired ($N = 10000$).

$$\min_{x_c \in D} J(x_c) \tag{23}$$

$$J(x_c) = \{J_1(x_c), J_2(x_c), J_3(x_c)\} \tag{24}$$

TABLE 4. Performance of the selected models (P_A, P_B, P_C) on the Pareto front in Figure 5.

$J(x_m)$	Point P_A	Point P_B	Point P_C
$J_1(x_m)$	**0.0945**	0.1399	0.0986
$J_2(x_m)$	0.1152	**0.0843**	0.0879

$$J_1(x_c) = [IAE]_1 = T_s \sum_{k=1}^{N} |P_{1\,ref}(k) - P_1(k)| \quad (25)$$

$$J_2(x_c) = [IAE]_2 = T_s \sum_{k=1}^{N} |P_{2\,ref}(k) - P_2(k)| \quad (26)$$

$$J_3(x_c) = [IADU]_{system} = \sum_{k=1}^{N} |u_{control}(k) - u_{control}(k-1)| \quad (27)$$

The decision vector is composed of the tuning parameters of the controllers, as shown in (28)-(29).

$$x_c = \{K_{p1}, K_{i1}, K_{p2}, K_{i2}\} \quad (28)$$

$$\underline{\mathbf{x}}_c \leq \mathbf{x}_c \leq \overline{\mathbf{x}}_c \quad (29)$$

The bounds of the decision space are shown in Table (3), which were determined based on the reference controllers with the linearized models of the system (the multi-objective optimization approach was applied to the nonlinear model of the system).

V. RESULTS AND DISCUSSION

The *ev*-MOGA algorithm was used to identify models that satisfactorily represent the dynamics of the air pressure system and tune the PI controllers [11]. For both cases, the optimization process (multi-objective optimization stage) was carried out on a hardware platform with an Intel Core i7 4700MQ processor at 2.4GHz and 12GB of RAM. The *Level Diagram* tool was used in the visualization and analysis stage of the Pareto fronts of each MOP [13], [42].

A. AIR PRESSURE SYSTEM IDENTIFICATION USING MULTI-OBJECTIVE OPTIMIZATION

For model identification, a pseudorandom binary sequence (PRBS) signal was applied to pneumatically actuate the input regulating valve (see Figure 3). It is important to note that the identification was performed on the nonlinear model of the system shown in (9)-(14), and the identified parameters have a physical interpretation. This ensures to some extent the operation of the system in different operating ranges.

Figure 5 shows the Pareto front obtained from the multi-objective optimization process using the *Level Diagram* tool. Each point on the front represents an optimal solution (a possible system model). The ∞-norm was selected to analyze the trade-offs that occur between design objectives $J_1(x_m)$ and $J_2(x_m)$. An increase in this norm directly reveals a worsening of at least one of the objectives of the proposed MOP. Each design objective can
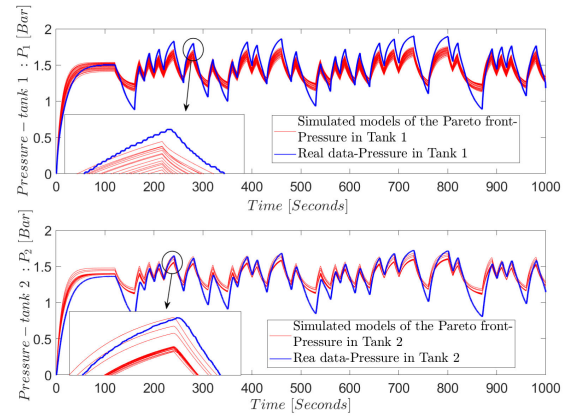
FIGURE 6. Models identified for pressures P_1 and P_2 of the air pressure system.
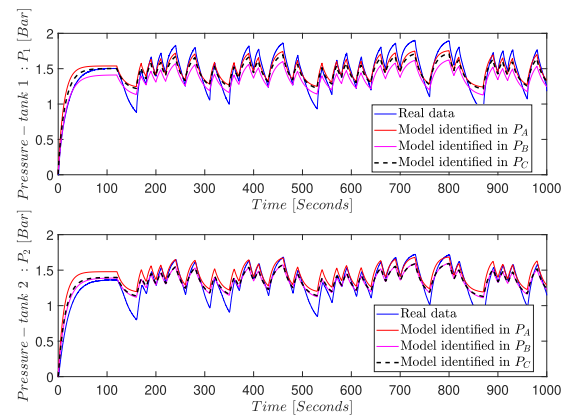
FIGURE 7. Models identified in the Pareto front of Figure 5, (P_A, P_B, P_C) to characterize the dynamics of the air pressure system.

be analyzed and visualized independently and synchronously on the Pareto front. This helps the designer to select the best solution for each MOP according to their preferences.

The Pareto front has been divided into two zones (A and B), and each point on the front represents a model with different performances or characteristics to describe the system's dynamics. Additionally, three points on the Pareto front (P_A, P_B, P_C) were selected to show the different trade-offs between models belonging to each zone. P_A and P_B show a conflict between the models of pressures P_1 and P_2 since improving one implies worsening the other. Point P_A (zone A) represents the best model for characterizing the dynamics of pressure P_1 but also the worst for representing pressure P_2 (see Table 4 where, J_1 in $P_A < J_1$ in P_B, and J_1 in $P_A < J_1$ in P_C, moreover J_2 in $P_A > J_2$ in P_B and J_2 in $P_A > J_2$ in P_C).

Point P_B (zone B) represents the best model for pressure P_2 but also the worst model for pressure P_1 (see Table 4 that J_2 in $P_B < J_2$ in P_A). Point P_C represents a model with satisfactory performance for both pressures P_1 and P_2 (chosen as a compromise model) without being the best for either of them. P_A represents pressure P_1 better
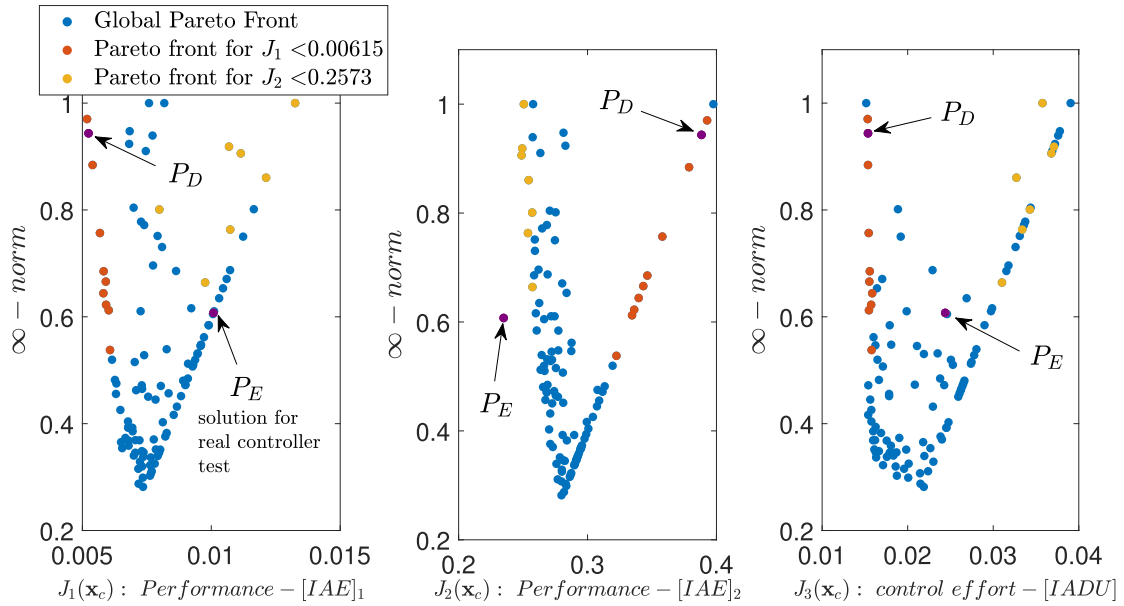

FIGURE 8. Pareto front representation of air pressure system controllers.
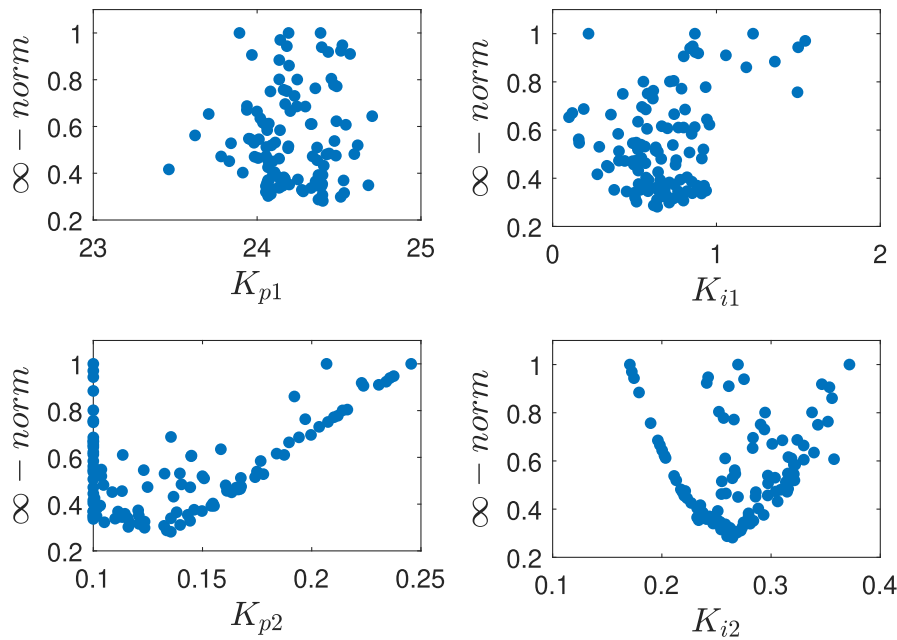

FIGURE 9. Tuning parameters of air pressure system controllers.

than P_C, and P_B represents pressure P_2 better than P_C. It is possible for a designer to select any of the models P_A, P_B, or P_C to represent the dynamics of the system under study. The choice of the model will be influenced by the designer's preferences. That is, if a designer prioritizes pressure P_1 over pressure P_2, the model to choose would be represented by P_A on the Pareto front (see Figure. 5). If, on the contrary, a designer prioritizes pressure P_2 over P_1, they should select the model represented by P_B on the Pareto front.

Finally, if a designer wishes to choose a model that, although not the best to represent pressures P_1 or P_2, can satisfactorily characterize both, they could choose any other point on the Pareto front. In this case, P_C was selected as the compromise model to represent the dynamics of the air pressure system. Figure 6 shows all identified models (21 models) for pressures P_1 and P_2 using a multi-objective optimization approach. In Figure 7, the system models represented on the Pareto front as P_A, P_B, and P_C are shown, and their performances are shown in Table 4.
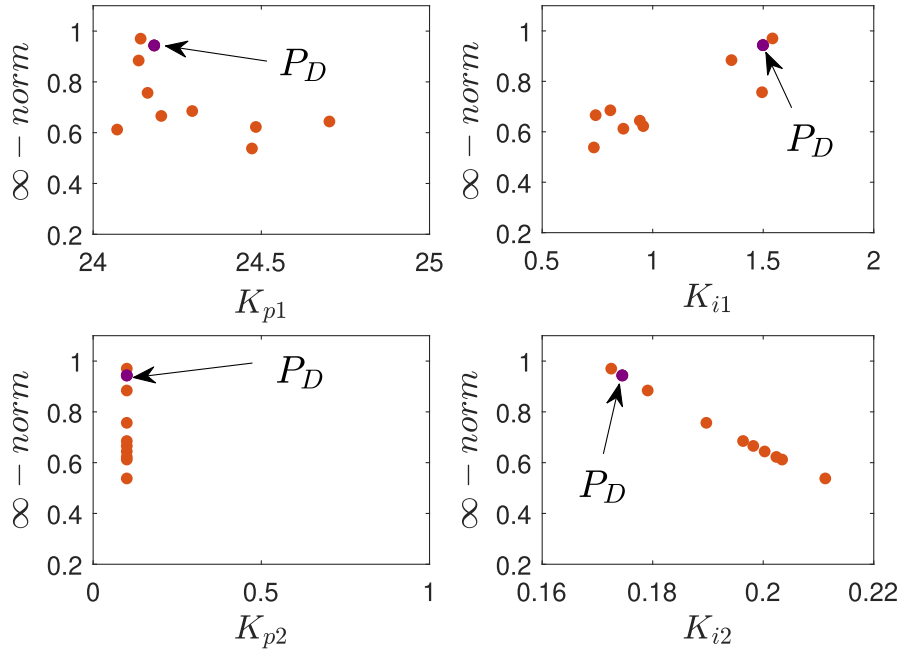
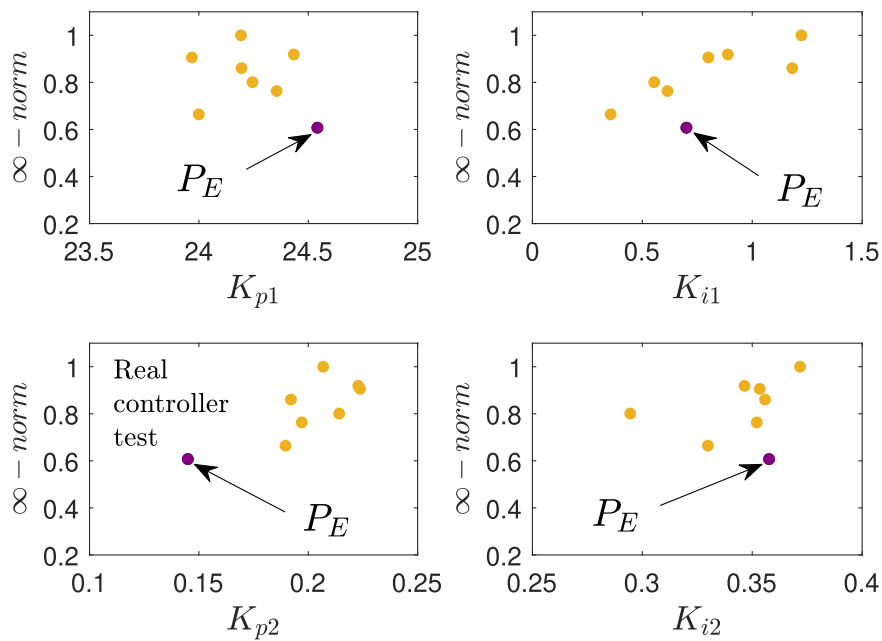**FIGURE 10.** Tuning parameters of air pressure system controllers for $J_1 < 0.00615$.

FIGURE 11. Tuning parameters of air pressure system controllers for $J_2 < 0.2573$.

TABLE 5. Performance of controllers in PD and PE of the Pareto front, with their tuning parameters.

Controllers	$J_1(x_c)$	$J_2(x_c)$	$J_3(x_c)$	K_{p1}	K_{i1}	K_{p2}	K_{i2}
P_D	**0.0052**	0.3884	**0.0154**	24.18	1.5	0.1	0.175
P_E	0.0101	**0.2349**	0.0244	24.54	0.71	0.15	0.358

Based on integrated absolute error (IAE), an acceptable range of errors in nonlinear models for real-world air pressure systems is typically around 5-10 % of the full-scale range [43]. Errors within this range ensure reliable system performance without significant deviation, maintaining control accuracy and operational efficiency. The model at point P_C is within the indicated range, as shown in Table 4.
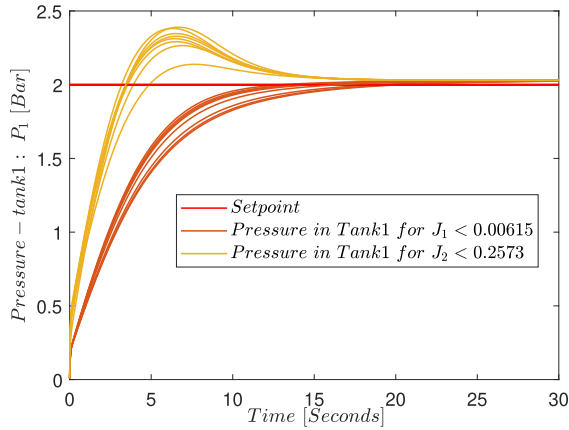
FIGURE 12. Responses of air pressure system PI controllers in tank 1 for $J_1 < 0.00615$, and $J_2 < 0.2573$.
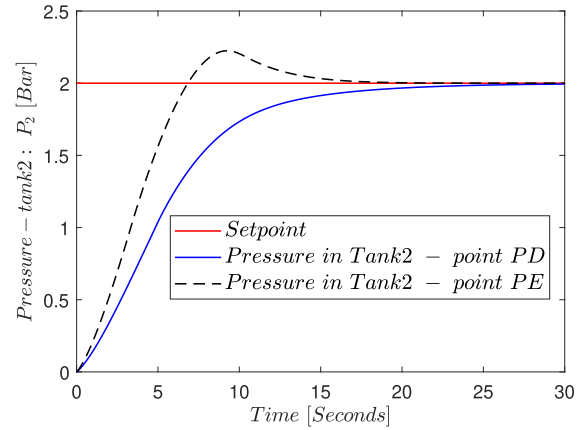

FIGURE 13. Responses of air pressure system PI controllers in tank 2 for $J_1 < 0.00615$, and $J_2 < 0.2573$.

FIGURE 14. Responses of air pressure system PI controllers in tank 1 for points PD, PE.
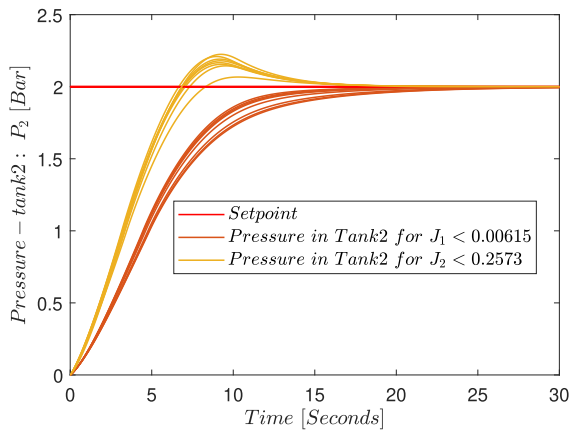

FIGURE 15. Responses of air pressure system PI controllers in tank 2 for points PD, PE.

FIGURE 16. Response real vs simulated of air pressure system PI controller in tank 1 for point PE.

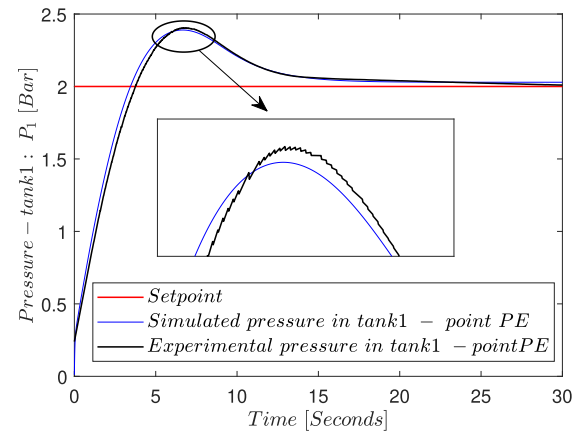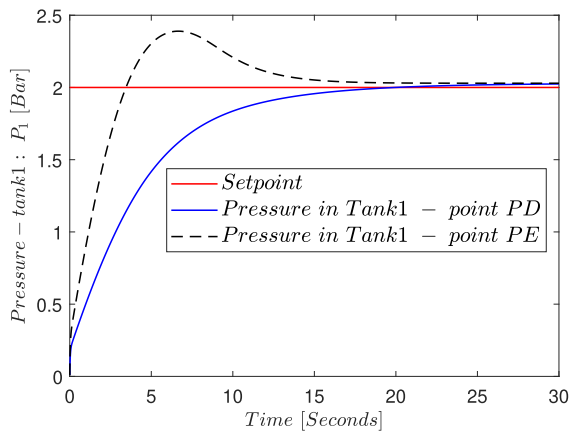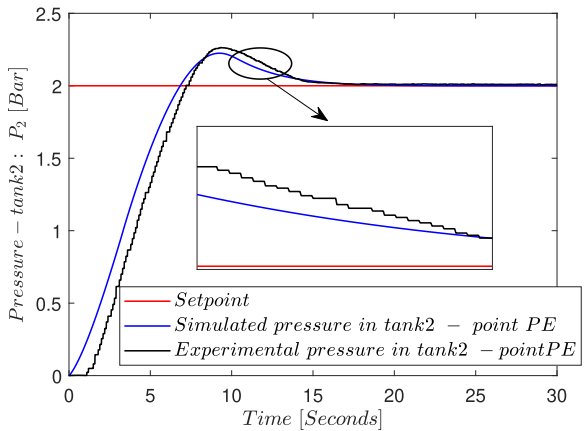**FIGURE 17.** Response real vs simulated of air pressure system PI controller in tank 2 for point PE.

B. AIR PRESSURE SYSTEM CONTROL USING MULTI-OBJECTIVE OPTIMIZATION

The optimization process was carried out to tune the PI controllers of the pressure system, and the Pareto front shown in Figure 8 was obtained. Objective $J_1(x_c)$ evaluates the quality of control for pressure P_1, objective $J_2(x_c)$ evaluates the quality of control for pressure P_2, and objective $J_3(x_c)$ evaluates the control action received by the system.

The tuning parameters of the Pareto front controller set are shown in Figure 9. Two regions of interest were established on the Pareto front (see Figure 8) to expand the multi-objective analysis. One region of interest (brown solutions) corresponds to the controllers with the best performance for

controlling pressure P_1, that is, when $J_1(x_c) < 0.00615$, and the other (yellow solutions) represents controllers with the best performance for controlling pressure P_2, that is, for $J_2(x_c) < 0.2573$.

In Figure 8, it is observed that both controller regions are in conflict because the best controllers for pressure P_1 are the worst for pressure P_2 (they are on opposite sides of the Pareto front) and vice versa. Similarly, the control actions for pressure P_1 are less drastic than those for pressure P_2. In Figures 10 and 11, the tuning parameter sets of the controllers for each selected region of interest on the Pareto front are visualized. Meanwhile, Figures 12 and 13 depict the responses of each set of controllers belonging to each region of interest.

For pressure P_1, the responses from the set of controllers where $J_1(x_c) < 0.00615$ (brown outputs) have a lower average IAE compared to the controllers where $J_2(x_c) < 0.2573$ (yellow outputs), (see Figure 12). For pressure P_2, the responses from the set of controllers where $J_2(x_c) < 0.2573$ (yellow outputs) have a lower average IAE compared to the controllers where $J_1(x_c) < 0.00615$ (brown outputs), (see Figure 13). A representative from each region of interest of the Pareto front of controllers was selected to quantify their performance and labeled as P_D and P_E. Table 5 shows the value of each design objective (performance) and its tuning parameters.

In Table 5, it can be observed that the controller in P_D exhibits better performance than the controller in P_E for regulating the pressure P_1 because $J_1(x_c)_{P_D} < J_1(x_c)_{P_E}$.

On the contrary, to regulate the pressure P_2, the controller in P_E performs better than the controller in P_D because $J_2(x_c)_{P_E} < J_2(x_c)_{P_D}$. Regarding control effort, it can be observed in Table 5 that for the controller in P_D, the objective $J_3(x_c)$ is lower than for the controller in P_E, meaning $J_3(x_c)_{P_D} < J_3(x_c)_{P_E}$.

In Figures 14 and 15, the responses of the controllers in P_D and P_E for pressures P_1 and P_2 respectively are shown. The P_E controller was chosen to conduct real tests in the pressure system, as it was prioritized for the control of pressure P_2 to stabilize more quickly and have a lower IAE compared to the P_D controller. Figures 16 and 17 display the real responses of the P_E controller for pressures P_1 and P_2 versus the simulated response. Section IV-B details the link to a video showing the plant in operation with the P_E controller.

VI. CONCLUSION

This paper presents a methodological approach based on multi-objective optimization to identify optimal models that characterize a system satisfactorily and determine optimal controllers that achieve its stabilization effectively. The framework applied in this paper follows the proposal shown in [14]. It is used in an experimental air pressure system to regulate two pressures, P_1 and P_2, with a single control input (underactuated and nonlinear system). A first multi-objective problem was proposed to identify models that satisfactorily represent the system dynamics. It could be analyzed

quantitatively and qualitatively that the models of both pressures were in conflict since the best model to represent one of the pressures is the worst to represent the other. According to the designer's preferences, a compromise model was chosen that adequately describes both pressures. Subsequently, another multi-objective problem was proposed to tune a set of optimal PI controllers to regulate each of the pressures in the system properly. A multi-objective analysis of the controller's performance was conducted according to the designer's preferences. That is, establishing to what extent one is willing to sacrifice one objective to gain another, a controller for the system was chosen (prioritizing the control of pressure P_2).

The compressed air system was operated with the selected controller, and its real response was compared with the simulated one. The multi-objective analysis done in this work facilitates the multidimensional understanding of the system's behavior, as it allows analyzing all required objectives without loss of information, which would be inevitable in a single-objective approach that consolidates all design objectives into one. Although it has a more complex decision stage, the knowledge of the possible solutions available to a designer compensates for this. Future work will focus on generating new nonlinear models to characterize the dynamics of the air pressure system and using different performance metrics to evaluate its behavior.

Finally, it is noted that the paper focuses on exploring to the fullest extent the possibilities offered by a multi-objective approach to meet certain design objectives that are in opposition and have been proposed by the designer, showing some available tools for multi-objective analysis to aid in the final decision-making process, rather than aiming to compare different control structures.

REFERENCES

[1] V. Huilcapi, R. Cajo, V. Ponguillo, and G. Gómez, "Educational platform for teaching automation and control engineering: A pneumatic levitation system," in *Proc. IEEE World Eng. Educ. Conf. (EDUNINE)*, Mar. 2023, pp. 1–6.

[2] B. Lima, R. Cajo, V. Huilcapi, and W. Agila, "Modeling and comparative study of linear and nonlinear controllers for rotary inverted pendulum," *J. Phys., Conf. Ser.*, vol. 783, Jan. 2017, Art. no. 012047.

[3] J. Zhang, "Design of a new PID controller using predictive functional control optimization for chamber pressure in a coke furnace," *ISA Trans.*, vol. 67, pp. 208–214, Mar. 2017.

[4] M. Liermann, "Pid tuning rule for pressure control applications," *Int. J. Fluid Power*, vol. 14, no. 1, pp. 7–15, Jan. 2013.

[5] J. Zhang, S. Zhang, Z. Dan, and C. Jiang, "Variable universe fuzzy PID control for multi-level gas tank pressure," in *Proc. IEEE 17th Int. Conf. Comput. Sci. Eng.*, Dec. 2014, pp. 1900–1904.

[6] H. Jianjun, T. Qianyuan, B. Yunpeng, and X. Degang, "Constrained generalized predictive control strategy for three-level air tank pressure system," in *Proc. 27th Chin. Control Decis. Conf. (CCDC)*, May 2015, pp. 404–409.

[7] J. liu, Y. Yang, S. Tan, and H. Wang, "Application of constrained multi-objective evolutionary algorithm in a compressed-air station scheduling problem," in *Proc. Chin. Control Conf. (CCC)*, Jul. 2019, pp. 2023–2028.

[8] N. Suwatanamala and N. Wongvanich, "Development of identification based fuzzy supervisory control for pressure tank system," in *Proc. 22nd Int. Conf. Control, Autom. Syst. (ICCAS)*, Nov. 2022, pp. 1410–1415.

[9] K. Bingi, R. Ibrahim, M. N. Karsiti, S. M. Hassan, and V. R. Harindran, "Real-time control of pressure plant using 2DOF fractional-order PID controller," *Arabian J. Sci. Eng.*, vol. 44, no. 3, pp. 2091–2102, Mar. 2019, doi: 10.1007/s13369-018-3317-9.

[10] V. Velmurugan, N. N. Praboo, and K. R. Kumar, "Performance evaluation of composite CRONE controller strategy for an air pressure system," *Math. Problems Eng.*, vol. 2023, pp. 1–15, Feb. 2023.

[11] J. M. Herrero, X. Blasco, M. Martínez, C. Ramos, and J. Sanchis, "Nonlinear robust identification of a greenhouse model using multi-objective evolutionary algorithms," *Biosyst. Eng.*, vol. 98, no. 3, pp. 335–346, Nov. 2007.

[12] U. Veyna, X. Blasco, J. M. Herrero, and A. Pajares, "Parameter uncertainty modeling for multiobjective robust control design. Application to a temperature control system in a proton exchange membrane fuel cell," *Eng. Appl. Artif. Intell.*, vol. 119, Mar. 2023, Art. no. 105758.

[13] X. Blasco, J. M. Herrero, J. Sanchis, and M. Martínez, "A new graphical visualization of n-dimensional Pareto front for decision-making in multiobjective optimization," *Inf. Sci.*, vol. 178, no. 20, pp. 3908–3924, Oct. 2008.

[14] V. Huilcapi, X. Blasco, J. M. Herrero, and G. Reynoso-Meza, "A loop pairing method for multivariable control systems under a multi-objective optimization approach," *IEEE Access*, vol. 7, pp. 81994–82014, 2019.

[15] G. R. Meza, X. Blasco, J. Sanchis, and J. M. Herrero, *Controller Tuning With Evolutionary Multiobjective Optimization: A Holistic Multiobjective Optimization Design Procedure*, vol. 85. Cham, Switzerland: Springer, 2016.

[16] C. M. Ionescu, C. F. Caruntu, R. Cajo, M. Ghita, G. Crevecoeur, and C. Copot, "Multi-objective predictive control optimization with varying term objectives: A wind farm case study," *Processes*, vol. 7, no. 11, p. 778, Oct. 2019.

[17] V. H. A. Ribeiro, G. Reynoso-Meza, and L. dos Santos Coelho, "Multiobjective optimization design procedures for data-driven unmanned aerial vehicles automatic target recognition systems," in *Unmanned Aerial Systems*. Amsterdam, The Netherlands: Elsevier, 2021, pp. 231–256.

[18] R. H. Stewart, T. S. Palmer, and B. DuPont, "A survey of multi-objective optimization methods and their applications for nuclear scientists and engineers," *Prog. Nucl. Energy*, vol. 138, Aug. 2021, Art. no. 103830.

[19] Y. Zheng and D. Wang, "A survey of recommender systems with multi-objective optimization," *Neurocomputing*, vol. 474, pp. 141–153, Feb. 2022.

[20] A. Pajares, X. Blasco, J. M. Herrero, and U. Veyna, "Advantages of using relevant nearly optimal solutions in multi-objective tuning of robust controllers," *ISA Trans.*, vol. 139, pp. 143–155, Aug. 2023.

[21] R. T. Marler and J. S. Arora, "Survey of multi-objective optimization methods for engineering," *Struct. Multidisciplinary Optim.*, vol. 26, no. 6, pp. 369–395, Apr. 2004.

[22] V. Pareto, A. S. Schwier, and A. N. Page, *Manual of Political Economy*. London, U.K.: Macmillan, 1972. [Online]. Available: https://catalogue.nla.gov.au/catalog/2742363

[23] K. Miettinen, *Nonlinear Multiobjective Optimization*, vol. 12. Cham, Switzerland: Springer, 2012.

[24] B. Y. Qu, Y. S. Zhu, Y. C. Jiao, M. Y. Wu, P. N. Suganthan, and J. J. Liang, "A survey on multi-objective evolutionary algorithms for the solution of the environmental/economic dispatch problems," *Swarm Evol. Comput.*, vol. 38, pp. 1–11, Feb. 2018.

[25] M. Lapucci and P. Mansueto, "Improved front steepest descent for multi-objective optimization," *Oper. Res. Lett.*, vol. 51, no. 3, pp. 242–247, May 2023.

[26] G. Cocchi, M. Lapucci, and P. Mansueto, "Pareto front approximation through a multi-objective augmented Lagrangian method," *EURO J. Comput. Optim.*, vol. 9, Jan. 2021, Art. no. 100008.

[27] X. Li, X. Li, K. Wang, and S. Yang, "A strength Pareto evolutionary algorithm based on adaptive reference points for solving irregular fronts," *Inf. Sci.*, vol. 626, pp. 658–693, May 2023.

[28] S. Petchrompo, D. W. Coit, A. Brintrup, A. Wannakrairot, and A. K. Parlikad, "A review of Pareto pruning methods for multi-objective optimization," *Comput. Ind. Eng.*, vol. 167, May 2022, Art. no. 108022.

[29] S. Wang, A. Zhou, B. Li, and P. Yang, "Differential evolution guided by approximated Pareto set for multiobjective optimization," *Inf. Sci.*, vol. 630, pp. 669–687, Jun. 2023.

[30] Y. Xu, H. Zhang, L. Huang, R. Qu, and Y. Nojima, "A Pareto front grid guided multi-objective evolutionary algorithm," *Appl. Soft Comput.*, vol. 136, Mar. 2023, Art. no. 110095.

[31] X. Wang, F. Zhang, and M. Yao, "A many-objective evolutionary algorithm with estimating the convexity-concavity of Pareto fronts and clustering," *Inf. Sci.*, vol. 644, Oct. 2023, Art. no. 119289.

[32] B.-C. Wang, Z.-Y. Shui, Y. Feng, and Z. Ma, "Evolutionary algorithm with dynamic population size for constrained multiobjective optimization," *Swarm Evol. Comput.*, vol. 73, Aug. 2022, Art. no. 101104.

[33] V. Huilcapi, B. Lima, X. Blasco, and J. M. Herrero, "Multi-objective optimization in modeling and control for rotary inverted pendulum," *RIAI-Revista Iberoamericana de Automatica e Inf. Ind.*, vol. 15, pp. 363–373, Jan. 2018. [Online]. Available: https://polipapers.upv.es/index.php/RIAI/issue/view/855/207

[34] H. Qiu, X. Xia, Y. Li, and X. Deng, "A dynamic multipopulation genetic algorithm for multiobjective workflow scheduling based on the longest common sequence," *Swarm Evol. Comput.*, vol. 78, Apr. 2023, Art. no. 101291.

[35] Z. Wang and A. Sobey, "A comparative review between genetic algorithm use in composite optimisation and the state-of-the-art in evolutionary computation," *Compos. Struct.*, vol. 233, Feb. 2020, Art. no. 111739.

[36] M. Wang, X. Li, and L. Chen, "An enhance multimodal multiobjective optimization genetic algorithm with special crowding distance for pulmonary hypertension feature selection," *Comput. Biol. Med.*, vol. 146, Jul. 2022, Art. no. 105536.

[37] G. Reynoso-Meza, J. Carrillo-Ahumada, V. H. Alves Ribeiro, and T. Marques, "Multi-objective PID controller tuning for multi-model control of nonlinear systems," *Social Netw. Comput. Sci.*, vol. 3, no. 5, p. 351, Jun. 2022.

[38] V. Huilcapi, X. Blasco, J. M. Herrero, A. Pajares, and G. Reynoso-Meza, "Application of an input-output pairings selection methodology to control multivariable systems based on multi-objective optimization," in *Proc. Int. Conf. Comput. Sci. Comput. Intell. (CSCI)*, Dec. 2021, pp. 443–449.

[39] H. Smedberg and S. Bandaru, "Interactive knowledge discovery and knowledge visualization for decision support in multi-objective optimization," *Eur. J. Oper. Res.*, vol. 306, no. 3, pp. 1311–1329, May 2023.

[40] K. Miettinen, "Survey of methods to visualize alternatives in multiple criteria decision making problems," *OR Spectr.*, vol. 36, no. 1, pp. 3–37, Jan. 2014.

[41] D. Nagar, P. Ramu, and K. Deb, "Visualization and analysis of Pareto-optimal fronts using interpretable self-organizing map (iSOM)," *Swarm Evol. Comput.*, vol. 76, Feb. 2023, Art. no. 101202.

[42] X. Blasco, J. M. Herrero, G. Reynoso-Meza, and M. A. M. Iranzo, "Interactive tool for analyzing multiobjective optimization results with level diagrams," in *Proc. Genetic Evol. Comput. Conf. Companion*, 2017, pp. 1689–1696.

[43] T. O. Hodson, "Root mean square error (RMSE) or mean absolute error (MAE): When to use them or not," *Geosci. Model Develop. Discuss.*, vol. 2022, pp. 1–10, Jul. 2022.

VÍCTOR HUILCAPI received the B.S. degree in electronic engineering and the M.Sc. degree in automation and industrial control from Escuela Superior Politécnica del Litoral (ESPOL), Guayaquil, Ecuador, in 2002 and 2015, respectively, and the Ph.D. degree from Universitat Politècnica de València (UPV), Spain, in 2021. He is currently an Associate Professor with Universidad Politécnica Salesiana (UPS). His main research interests include the control and modeling of multivariable systems, process optimization, and multiobjective optimization techniques applied to engineering.

CHRISTIAN CASTILLO received the degree in industrial automation engineering from Escuela Superior Politécnica del Litoral, Guayaquil, Ecuador. He is currently an Industrial Networks Consultant, where he is involved in the process automation area. His academic background includes activities related to the design of industrial networks and awareness of OT systems and the respective IT/OT convergence applying standards, such as IEC/ISA 62443 from manufacturing to utilities industry.

DANIEL SANCHEZ received the bachelor's degree in electronic and automation engineering from Escuela Superior Politécnica del Litoral, Guayaquil, Ecuador. He is currently an Engineering Assistant in the field of electrical engineering. He has been involved in electrical projects for food and beverage companies, such as the mounting and installation of boilers and the design of electrical boards. His primary research interests include renewable energy, programming PLC, and the electrical field.

RICARDO CAJO received the M.Sc. degree in industrial automatic control from Escuela Superior Politécnica del Litoral (ESPOL), Guayaquil, Ecuador, and the Ph.D. degree in engineering from Ghent University. He is currently a University Lecturer with ESPOL in the field of electronics and automation engineering. His academic background is complemented by a notable research activity, reflected in various scientific publications in journals, conferences, and book chapters. In addition, he has played a crucial role as a Reviewer in high-impact journals, such as IEEE Transactions on Systems, Man and Cybernetics: Systems, IEEE Transactions on Aerospace and Electronic Systems, IEEE Systems Journal, and IEEE Transactions on Cybernetics. His primary research interests include control of autonomous vehicles, such as UAVs, UGVs, and USVs, as well as fractional-order control (FOC) systems, multi-agent systems, and model-based predictive control.

● ● ●